

# Edge-Local and Qubit-Efficient Quantum Graph Learning for the NISQ Era

Armin Ahmadvaniha

ahmadvaniha@mcmaster.ca

Jake Doliskani

jake.doliskani@mcmaster.ca

Department of Computing and Software, McMaster University

## Abstract

Graph neural networks (GNNs) are a powerful framework for learning representations from graph-structured data, but their direct implementation on near-term quantum hardware remains challenging due to circuit depth, multi-qubit interactions, and qubit scalability constraints. In this work, we introduce a fully quantum graph convolutional architecture designed explicitly for unsupervised learning in the noisy intermediate-scale quantum (NISQ) regime.

Our approach combines a variational quantum feature extraction layer with an edge-local and qubit-efficient quantum message-passing mechanism inspired by the Quantum Alternating Operator Ansatz (QAOA) framework. Unlike prior models that rely on global operations or multi-controlled unitaries, our model decomposes message passing into pairwise interactions along graph edges using only hardware-native single- and two-qubit gates. This design reduces the qubit requirement from  $O(Nn)$  to  $O(n)$  for a graph with  $N$  nodes and  $n$ -qubit feature registers, enabling implementation on current quantum devices regardless of graph size. We train the model using the Deep Graph Infomax objective to perform unsupervised node representation learning. Experiments on the Cora citation network and a large-scale genomic SNP dataset demonstrate that our model remains competitive with prior quantum and hybrid approaches.

**keywords:** Genomic, Quantum Graph Convolutional Neural Network, Quantum Machine Learning, Unsupervised Learning

## 1 Introduction

Graph-structured data arise naturally across many scientific domains, including social networks, molecular chemistry, genomics, and citation analysis. In recent years, machine learning methods—particularly graph neural networks (GNNs)—have become a standard tool for extracting meaningful representations from such data, enabling tasks such as classification, clustering, and unsupervised representation learning [18, 11, 27, 12, 35, 26]. At the same time, advances

in deep learning have demonstrated remarkable success in vision, language, and scientific discovery, further motivating the development of expressive models for structured data [19, 17, 23].

Despite this success, learning effective representations for large, high-dimensional graphs remains computationally demanding. Classical graph neural networks rely on repeated aggregation and transformation of node features, which can become costly as graph size and feature dimensionality grow. These challenges have motivated interest in alternative computational paradigms that may offer new ways to represent and process complex, structured data.

One such paradigm is quantum computing. The emergence of quantum hardware has raised the prospect of accelerating or enhancing certain machine learning tasks by exploiting high-dimensional quantum state spaces and quantum interference effects. This has led to the rapidly growing field of quantum machine learning (QML), which investigates the use of parameterized quantum circuits as trainable models for classical or quantum data [4, 30, 10, 15]. However, current quantum hardware operates in the noisy intermediate-scale quantum (NISQ) regime, characterized by limited qubit counts, short coherence times, and restricted circuit depth. As a result, practical QML algorithms must be designed to be shallow, noise-tolerant, and compatible with hardware-native gate sets [6, 22, 3].

These constraints are particularly challenging for graph learning. Classical graph convolutional networks (GCNs) rely on message passing driven by the adjacency structure of the graph, repeatedly aggregating information from neighboring nodes through linear transformations and nonlinearities [18, 12, 14]. Translating this paradigm directly to the quantum setting is challenging: encoding graph structure into quantum circuits typically requires multi-qubit interactions, conditional operations, or high-depth constructions that scale poorly with graph size. As a result, naive quantum analogues of GCNs quickly exceed the capabilities of NISQ-era devices.

Several quantum graph learning models have been proposed in recent years. Early work introduced quantum graph neural networks in which graph structure is encoded through

Hamiltonian-based variational evolutions [33]. Subsequent approaches developed quantum graph convolutional architectures inspired by classical GCNs, demonstrating promising performance on graph-level classification tasks [38, 39, 36]. Other architectural variants have explored symmetry-aware and equivariant graph constructions [21].

However, many of these models either assume idealized quantum hardware, rely on global operations over all nodes, or require circuit components—such as multi-controlled unitaries—that are prohibitively expensive on near-term devices [16, 8]. In particular, an  $n$ -controlled unitary gate requires  $O(n^2)$  two-qubit gates without ancilla qubits, and still  $O(n)$  two-qubit gates even with  $O(n)$  ancilla, making such constructions highly sensitive to noise and compilation overhead [2].

To mitigate these limitations, a range of hybrid quantum-classical graph learning approaches have been explored. Such models typically integrate quantum circuits as components within broader classical pipelines, often relying on substantial classical pre- or post-processing relative to the quantum subroutine [1, 7, 31, 25]. These hybrid decompositions reduce quantum resource requirements and facilitate near-term implementation, particularly in supervised learning settings where labeled data provide a strong training signal.

However, while hybrid models alleviate hardware constraints by shifting a substantial portion of computation to the classical domain, they may limit the extent to which relational structure is processed coherently within the quantum circuit. In particular, in hybrid architectures where quantum circuits are used primarily for local feature extraction and classical algorithms perform neighborhood aggregation, the relational message-passing mechanism remains entirely classical. When such classical aggregation operators are applied repeatedly to *low-dimensional embeddings* produced by quantum encoders, the resulting representations may be prone to oversmoothing, leading to a loss of discriminative information across graph neighborhoods.

**Our contribution.** In this work, we present a fully quantum graph convolutional framework designed explicitly for unsupervised learning on NISQ-era hardware. Our approach replaces global, hardware-intensive message-passing operations with a qubit-efficient, edge-local quantum message-passing mechanism inspired by the Quantum Alternating Operator Ansatz (QAOA) [9, 13]. The model consists of two key components: a variational quantum feature extraction circuit applied independently to each node, and a quantum message-passing layer that encodes graph structure via alternating local interactions between pairs of neighboring nodes.

Crucially, our design avoids multi-controlled unitaries altogether and relies exclusively on elementary, hardware-native gates such as single-qubit rotations and two-qubit entangling operations. By applying message passing edge-by-edge rather than globally, the overall algorithm requires

only a constant number of qubits at any point in time, while maintaining gate complexity comparable to existing quantum graph learning models. This makes our model directly implementable on current quantum processors, regardless of graph size.

We evaluate our model on two representative datasets: the Cora citation network and a large-scale genomic single nucleotide polymorphism (SNP) dataset. Using the Deep Graph Infomax objective for unsupervised representation learning [32], we demonstrate that our fully quantum model learns meaningful and discriminative node embeddings. Moreover, compared to a hybrid quantum-classical baseline that we implemented using classical message passing, our model exhibits a clear advantage in preserving semantic structure in unsupervised settings, highlighting the importance of fully quantum message passing for graph representation learning.

The source code for our implementation is publicly available at <https://github.com/ArminAhmadkhaniha/QGCNlib>.

## 2 Preliminaries

### 2.1 Qubits and Quantum Circuits

A *qubit* is the basic unit of quantum information. A qubit state is a vector in a two-dimensional complex Hilbert space  $\mathbb{C}^2$  [34]. The two computational basis states are written using Dirac notation as  $|0\rangle$  and  $|1\rangle$ :

$$|0\rangle = \begin{bmatrix} 1 \\ 0 \end{bmatrix}, \quad |1\rangle = \begin{bmatrix} 0 \\ 1 \end{bmatrix}$$

Any valid qubit state  $|\psi\rangle$  is a linear combination of these basis states with complex coefficients  $\alpha$  and  $\beta$ :

$$|\psi\rangle = \alpha|0\rangle + \beta|1\rangle, \quad \text{where } |\alpha|^2 + |\beta|^2 = 1$$

When we consider multiple qubits, their joint state lies in the tensor product of their Hilbert spaces. For example, the state of two qubits lives in  $\mathbb{C}^2 \otimes \mathbb{C}^2 = \mathbb{C}^4$ .

Quantum states are evolved by applying *unitary operators*. An operator  $U$  is unitary if  $U^\dagger U = I$ , where  $U^\dagger$  is the Hermitian conjugate. The evolution  $|\psi_1\rangle \rightarrow |\psi_2\rangle$  of quantum states is given by  $|\psi_2\rangle = U|\psi_1\rangle$ . Quantum gates are unitary operations that act on one or more qubits. By applying a sequence of such gates to an initial state, we form a *quantum circuit*. Any unitary operator can be considered as a rotation. In particular, single-qubit unitaries are described by a set of angles. In quantum machine learning, a quantum circuit prepares a state  $|\psi_\theta\rangle$  by acting on a known input state, usually  $|0\rangle^{\otimes n}$ , using gates parameterized by angles  $\theta$ . After preparing a quantum state, we can extract classical information by measurement. In our case, we often measure expectation values of observables such as the Pauli-Z operator. The expectation

value of  $Z$  with respect to a qubit  $|\psi_\theta\rangle$  is:

$$\langle Z \rangle = \langle \psi_\theta | Z | \psi_\theta \rangle.$$

If a circuit includes parameterized rotation gates, such as  $R_X(\theta)$  or  $R_Y(\theta)$  introduced below, then the output state  $|\psi_\theta\rangle$  depends on tunable parameters  $\theta$ . To train a model, we compute gradients of the measured value with respect to these parameters and update them using classical optimization methods. A variational quantum circuit (VQC) consists of an input encoding, a parameterized unitary  $U(\theta)$ , and a measurement step. The parameters  $\theta$  are updated iteratively to minimize a classical loss function [29]. This is the basis of most quantum machine learning algorithms. We use the same approach in this work.

**Basic Quantum Gates and Operators** In our quantum circuit designs, we make frequent use of the standard elementary quantum gates. We briefly describe these gates in the following.

- Pauli's X, Y, and Z operators:

$$X = \begin{bmatrix} 0 & 1 \\ 1 & 0 \end{bmatrix}, \quad Y = \begin{bmatrix} 0 & -i \\ i & 0 \end{bmatrix}, \quad Z = \begin{bmatrix} 1 & 0 \\ 0 & -1 \end{bmatrix}$$

- The Hadamard gate:

$$H = \frac{1}{\sqrt{2}} \begin{bmatrix} 1 & 1 \\ 1 & -1 \end{bmatrix}$$

- The cNOT gate:

$$\text{cNOT} = \begin{bmatrix} 1 & 0 & 0 & 0 \\ 0 & 1 & 0 & 0 \\ 0 & 0 & 0 & 1 \\ 0 & 0 & 1 & 0 \end{bmatrix}$$

- Single-qubit rotation gates:

$$\begin{aligned} R_X(\theta) &= e^{-i\theta X/2} = \cos(\theta/2)I - i \sin(\theta/2)X \\ R_Y(\theta) &= e^{-i\theta Y/2} = \cos(\theta/2)I - i \sin(\theta/2)Y \\ R_Z(\theta) &= e^{-i\theta Z/2} = \cos(\theta/2)I - i \sin(\theta/2)Z \end{aligned}$$

A general single-qubit unitary with learnable parameters  $(\alpha, \beta, \gamma)$  is defined as:

$$R(\alpha, \beta, \gamma) = R_Z(\alpha)R_Y(\beta)R_Z(\gamma).$$

In matrix form,  $R(\alpha, \beta, \gamma)$  can be expressed as

$$R(\alpha, \beta, \gamma) = \begin{bmatrix} e^{-\frac{i(\alpha+\gamma)}{2}} \cos\left(\frac{\beta}{2}\right) & -e^{-\frac{i(\alpha-\gamma)}{2}} \sin\left(\frac{\beta}{2}\right) \\ e^{\frac{i(\alpha-\gamma)}{2}} \sin\left(\frac{\beta}{2}\right) & e^{\frac{i(\alpha+\gamma)}{2}} \cos\left(\frac{\beta}{2}\right) \end{bmatrix}.$$

## 2.2 Graph Convolutional Neural Networks (GCNs)

The graph convolutional network (GCN) model used in this work is based on the formulation introduced by Kipf and Welling [18]. Given a graph  $G = (V, E)$  with  $N$  nodes, feature matrix  $X \in \mathbb{R}^{N \times d}$ , and adjacency matrix  $A \in \{0, 1\}^{N \times N}$ , the forward propagation rule for a single GCN layer is defined as

$$H^{(l+1)} = \sigma(D^{-1/2} \tilde{A} D^{-1/2} H^{(l)} W^{(l)}) \quad (1)$$

where  $\tilde{A} = A + I$  is the adjacency matrix with self-loops,  $D$  is the corresponding degree matrix,  $H^{(0)} = X$ ,  $W^{(l)} \in \mathbb{R}^{d \times d}$  is the trainable weight matrix at layer  $l$ , and  $\sigma$  is a nonlinear activation function.

The term  $H^{(l)} W^{(l)}$  performs a learnable feature transformation, while the normalized adjacency matrix  $D^{-1/2} \tilde{A} D^{-1/2}$  encodes the graph structure and propagates information between neighboring nodes. Thus, each layer simultaneously aggregates local neighborhood information and updates node representations.

Stacking multiple such layers yields embeddings for each node that combine its own features with those of its neighbors. These representations can then be used for downstream tasks such as classification, clustering, or unsupervised learning with mutual information objectives.

## 3 A Fully Quantum GCN

Let  $G = (V, E)$  be the input graph with  $N$  nodes, adjacency matrix  $A \in \{0, 1\}^{N \times N}$ , and node feature matrix  $X \in \mathbb{R}^{N \times d}$ , where each row represents the features of a single node. Our proposed quantum graph learning algorithm consists of three main components:

1. Quantum feature extraction via a variational quantum circuit,
2. A single-layer quantum message passing unitary acting as a graph-structured message-passing operation,
3. An unsupervised Deep Graph Infomax (DGI) objective applied to the resulting node embeddings.

We describe each of these components in detail in the following sections.

### 3.1 Quantum Feature Extraction

Let  $\mathbf{x} = (x_0, x_1, \dots, x_{d-1})$  be any row of the feature matrix  $X$ . Then  $\mathbf{x}$  can be expressed as a quantum state using amplitude encoding [20] as follows. Let  $n = \lceil \log d \rceil$ . Using amplitude encoding on  $n$  qubits, we prepare the state

$$|\psi_{\mathbf{x}}\rangle = \frac{1}{\|\mathbf{x}\|} \sum_{j=0}^{d-1} x_j |j\rangle.$$

To extract features, we apply a variational circuit consisting of  $L$  layers of an entangling block, for some  $L \geq 1$ . Such circuits alternate single-qubit rotations with entangling gates. For example, following Schuld *et al.* [28], an entangling block consists of a layer of single-qubit rotation gates applied to each qubit, followed by a layer of controlled two-qubit gates connecting qubit pairs at a fixed range. Denoting by  $C_c(U_t)$  a controlled- $U$  gate with control qubit  $c$  and target qubit  $t$ , such a block can be written as

$$B = \prod_{k=0}^{\lfloor n/r \rfloor - 1} C_{c_k}(U_{t_k}) \prod_{j=0}^{n-1} U_j. \quad (2)$$

Here, the qubit pairs  $(c_k, t_k)$  depend on the range parameter  $r$ , which can take values  $r = 1, 2, \dots, n$ .

In practice, we use  $Z$ -rotations  $R_Z(\gamma_j)$  or general  $R(\alpha_j, \beta_j, \gamma_j)$  gates on each qubit, followed by CNOT (or CZ) gates entangling qubit  $k$  with qubit  $(k+r) \bmod n$ . In this case, the block  $B$  is expressed as

$$B(\theta) = \prod_{k=0}^{\lfloor n/r \rfloor - 1} \text{CNOT}_{k, (k+r) \bmod n} \prod_{j=0}^{n-1} R(\alpha_j, \beta_j, \gamma_j),$$

where  $\theta$  denotes the set of parameters  $(\alpha_j, \beta_j, \gamma_j)$  for  $j = 0, \dots, n-1$ . Applying  $L$  layers of the unitary  $B$  with (possibly different) parameter sets  $\theta_1, \theta_2, \dots, \theta_L$ , the complete entangling unitary is

$$U_{\text{ent}}(\theta) = B(\theta_L)B(\theta_{L-1}) \cdots B(\theta_1).$$

The resulting state  $|\psi_L(\theta)\rangle = U_{\text{ent}}(\theta)|\psi_x\rangle$  encodes the input node features into an entangled quantum state.

Finally, the classical encoding of the node  $\mathbf{x}$  is obtained by computing the Pauli- $Z$  expectation values on each qubit of  $|\psi_L(\theta)\rangle$ . Denoting the expectation value of qubit  $i$  by  $h_i$ , the encoding is stored as the vector

$$\mathbf{h} = (h_0, \dots, h_{n-1}) \in \mathbb{R}^n. \quad (3)$$

Figure 1 shows a 5-qubit entangling unitary circuit  $U_{\text{ent}}$  for a single layer ( $L = 1$ ) and the final measurements.

## 3.2 Quantum Message Passing

In this section, we formulate a quantum analogue of classical message passing by adapting the alternating-operator structure of the Quantum Alternating Operator Ansatz (QAOA), a framework for constructing parameterized quantum circuits for combinatorial optimization and constraint-satisfaction problems. It was originally introduced by Farhi, Goldstone, and Gutmann [9] as a quantum algorithm for approximate optimization, and later generalized by Hadfield *et al.* [13] into a flexible ansatz applicable to a broad class of problems. While QAOA is traditionally employed for global combinatorial optimization, its alternating ansatz of *cost* and *mixer*

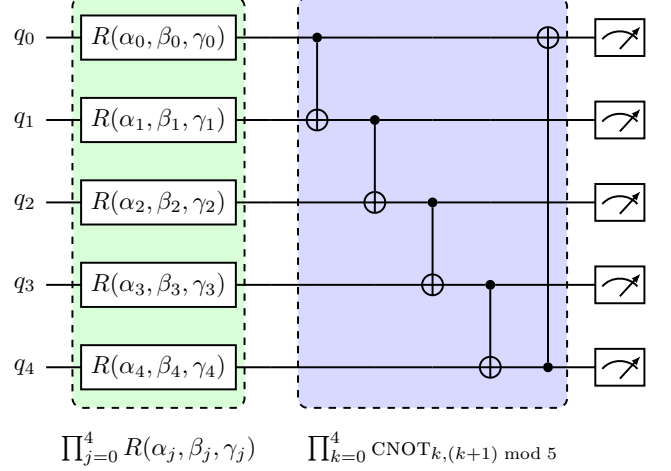


Figure 1: Five-qubit quantum feature extraction for a single layer of the unitary  $B$  defined in (2).

Hamiltonians provides a rigorous framework for inducing graph-structured state evolution. In the following, we first briefly review the QAOA framework, and then instantiate the general operators to obtain circuits that decompose into local operators and can be efficiently implemented.

### 3.2.1 The QAOA framework

At a high level, QAOA alternates between two families of unitary operators: *problem* (or phase-separation) operators, which encode the objective function, and *mixing* operators, which drive transitions between candidate solutions. This alternating structure defines both the expressivity and the algorithmic intuition behind QAOA.

Formally, a depth- $p$  QAOA circuit prepares a quantum state of the form

$$|\psi(\gamma, \beta)\rangle = \prod_{k=1}^p (e^{-i\beta_k H_M} e^{-i\gamma_k H_C}) |\psi_0\rangle,$$

where  $H_C$  is the *problem* (or cost) Hamiltonian, typically diagonal in the computational basis and encoding the cost function,  $H_M$  is the *mixing* Hamiltonian,  $|\psi_0\rangle$  is an initial state (often the uniform superposition), and  $\gamma = (\gamma_1, \dots, \gamma_p)$  and  $\beta = (\beta_1, \dots, \beta_p)$  are real parameters optimized by a classical outer loop. The general QAOA circuit is shown in Figure 2.

In the original formulation of QAOA for problems such as Max-Cut, the mixing Hamiltonian is chosen as  $H_M = \sum_i X_i$ , corresponding to global bit-flip operations, while  $H_P$  is derived directly from the objective function of the instance. The generalized Quantum Alternating Operator Ansatz relaxes these choices by allowing problem-specific design of both operators. In particular, the mixing operator need not be a sum of Pauli- $X$  terms, and may be constructed to preserve

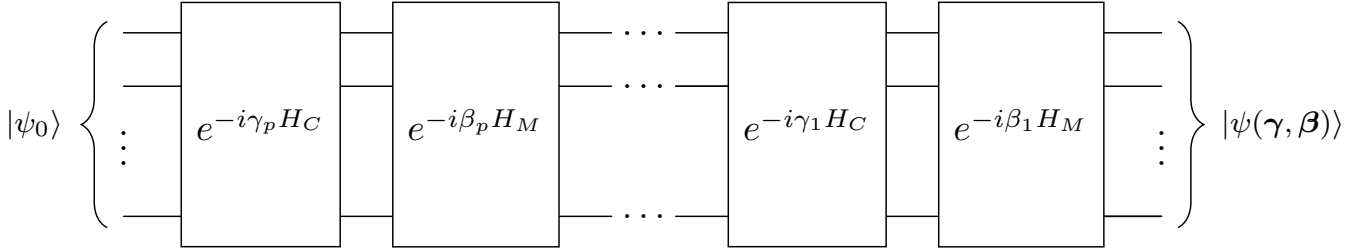


Figure 2: General QAOA circuit with input  $|\psi_0\rangle$  and parameter sets  $(\beta_1, \dots, \beta_p)$  and  $(\gamma_1, \dots, \gamma_p)$ .

hard constraints or to respect the structure of the feasible solution space.

From a conceptual perspective, QAOA can be interpreted in several complementary ways. It may be viewed as a digitized version of adiabatic quantum optimization, where increasing the depth  $p$  yields progressively better approximations to continuous adiabatic evolution. It can also be understood as a variational quantum algorithm, or as a quantum analogue of classical local search or message-passing procedures, in which alternating operators play distinct and complementary roles.

A key practical feature of QAOA is that both the problem and mixing unitaries can often be decomposed into local quantum gates, such as single-qubit rotations and two-qubit controlled-phase operations. This locality makes QAOA particularly well-suited for implementation on near-term quantum hardware.

### 3.2.2 An edge-local quantum message passing

We propose a quantum analogue of classical message passing based on QAOA. Given the graph  $G = (V, E)$ , we define the cost Hamiltonian as

$$H_C = \sum_{(u,v) \in E} \sum_{k=0}^{n-1} Z_{uk} Z_{vk}, \quad (4)$$

where  $Z_{uk}$  denotes the Pauli- $Z$  operator acting on the  $k$ -th feature qubit associated with node  $u$ . The Hamiltonian  $H_C$  induces pairwise interactions between neighboring nodes, acting feature-wise across each edge of the graph. The mixer Hamiltonian is defined as

$$H_M = \sum_{u \in V} \sum_{k=0}^{n-1} X_{uk}, \quad (5)$$

where  $X_{uk}$  denotes the Pauli- $X$  operator acting on the  $k$ -th feature qubit of node  $u$ . The mixer acts locally on each node's feature register and redistributes amplitude among feature configurations. Alternating applications of the unitaries  $e^{-i\gamma H_C}$  and  $e^{-i\beta H_M}$  define a layered quantum evolution analogous to iterative message passing. The cost Hamiltonian  $H_C$  encodes interactions between neighboring nodes

by introducing feature-dependent phases, while the mixer Hamiltonian  $H_M$  enables the propagation of this information through interference across the local feature space. Increasing the circuit depth corresponds to multiple rounds of quantum message passing on the underlying graph.

Hamiltonians of this form have appeared previously in the context of quantum graph optimization problems [13]. To the best of our knowledge, however, this is the first use of such an alternating-operator construction as a quantum message-passing mechanism for learning on graphs.

From the above Hamiltonians, the message-passing unitary corresponding to a single QAOA layer with parameters  $\beta$  and  $\gamma$  is given by

$$U_{\text{MP}}(\gamma, \beta) = e^{-i\beta H_M} e^{-i\gamma H_C} = \prod_{u \in V} \prod_{k=0}^{n-1} R_{X_{uk}}(2\beta) \prod_{(u,v) \in E} \prod_{k=0}^{n-1} e^{-i\gamma Z_{uk} Z_{vk}},$$

where  $R_{X_{uk}}(\theta) = e^{-i\theta X_{uk}/2}$ . The second equality follows from the fact that the operators  $Z_{uk} Z_{vk}$  commute for different  $(u, v) \in E$  and different feature indices  $k$ , and similarly the operators  $X_{uk}$  commute for different nodes  $u \in V$  and feature indices  $k$ .

Each component of the unitary  $U_{\text{MP}}$  can be efficiently implemented using standard quantum gates. The unitary  $R_{X_{uk}}(2\beta)$  is a single-qubit rotation applied to the  $k$ -th feature qubit associated with node  $u$ .

The two-qubit unitaries  $e^{-i\gamma Z_{uk} Z_{vk}}$  admit an efficient decomposition in terms of CNOT and single-qubit rotation gates. Specifically, for each edge  $(u, v) \in E$  and feature index  $k$ , we may write

$$e^{-i\gamma Z_{uk} Z_{vk}} = \text{CNOT}_{uk \rightarrow vk} \cdot R_{Z_{vk}}(2\gamma) \cdot \text{CNOT}_{uk \rightarrow vk}, \quad (6)$$

where

- $\text{CNOT}_{uk \rightarrow vk}$  denotes a CNOT gate with control qubit  $uk$  and target qubit  $vk$ .
- $R_{Z_{vk}}(2\gamma)$  is a single qubit rotation applied to the feature qubit  $k$  of the node  $v$ .

The circuit complexity of the unitary  $U_{\text{MP}}$  constructed from the above gates scales linearly with the number of input qubits. More precisely, the graph consists of  $N$  nodes, each represented by an  $n$ -qubit feature register, so the total number of qubits required is  $Nn$ . Since each feature qubit participates in a constant number of single- and two-qubit gates per layer, the gate complexity of a single message-passing layer is  $O(Nn)$ .

For a quantum computer with sufficient qubit resources, this scaling is nearly optimal. However, the simultaneous use of a large number of qubits becomes prohibitive on NISQ hardware. To address this limitation, we next propose a qubit-efficient variant of  $U_{\text{MP}}$  that follows the same underlying message-passing logic while significantly reducing the number of qubits required.

### 3.2.3 Edge-local and qubit-efficient

Consider an edge  $(u, v) \in E$  of the graph  $G$ . The action of the unitary  $U_{\text{MP}}$  restricted to this edge can be expressed as

$$U_{\text{MP},uv}(\gamma, \beta) := \prod_{k=0}^{n-1} R_{X_{uk}}(2\beta) \prod_{k=0}^{n-1} e^{-i\gamma Z_{uk}Z_{vk}}.$$

This unitary can be efficiently implemented using the decomposition described in (6). Figure 3 illustrates the corresponding circuit for  $U_{\text{MP},uv}(\gamma, \beta)$  in the case where each node is represented by an  $n = 4$  qubit feature register.

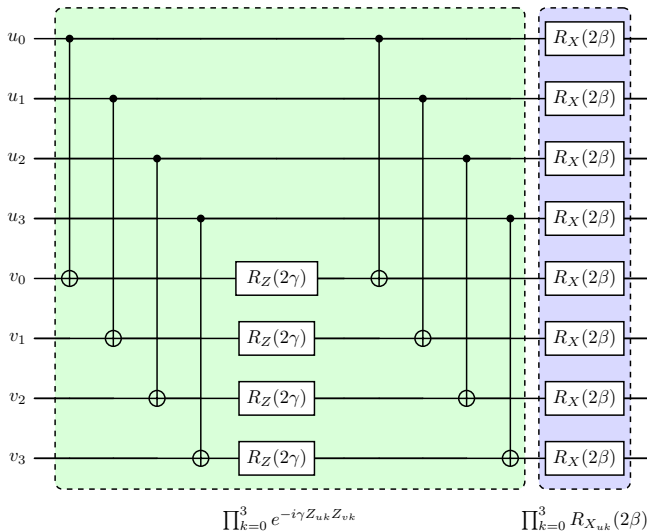


Figure 3: The quantum message-passing unitary  $U_{\text{MP},uv}(\gamma, \beta)$  for an edge  $(u, v)$ , where each node is represented by  $n = 4$  qubits.

The key idea behind our qubit-efficient construction is to apply the edge-local unitary  $U_{\text{MP},uv}$  separately for each edge  $(u, v) \in E$ , rather than implementing the full unitary  $U_{\text{MP}}$  on all nodes simultaneously. To obtain embeddings for all

nodes in  $G$ , we first apply the quantum feature extraction procedure of Section 3.1 to each node individually, producing an  $n$ -qubit feature encoding. We then iterate over the edges  $(u, v) \in E$ , and for each edge apply the unitary  $U_{\text{MP},uv}$  to the feature registers corresponding to nodes  $u$  and  $v$ . Measurement of the output yields updated embeddings for both nodes.

Crucially, at no point does this procedure require more than  $2n$  qubits simultaneously. The quantum feature extraction step uses  $n$  qubits, as it operates on one node at a time, while each application of  $U_{\text{MP},uv}$  uses  $2n$  qubits, acting only on the pair of nodes associated with a single edge.

For a concrete implementation of the above algorithm, we must address two practical questions:

- (i) After the quantum feature extraction step, each node is represented by an  $n$ -dimensional classical encoding. How should these encodings be mapped to quantum states for the quantum message-passing step?
- (ii) Since the quantum message-passing procedure iterates over edges, nodes with multiple neighbors will produce multiple embeddings. How can these be combined into a single embedding per node?

Both problems admit natural and efficient solutions. We address problem (i) using a standard data-encoding strategy from variational quantum algorithms, namely *angle encoding*. Given a vector  $\mathbf{h} = (h_0, h_1, \dots, h_{n-1}) \in \mathbb{R}^n$ , we encode  $\mathbf{h}$  into an  $n$ -qubit quantum state  $|\phi_{\mathbf{h}}\rangle$  by applying single-qubit rotations to the computational basis state:

$$|\phi_{\mathbf{h}}\rangle = \bigotimes_{k=0}^{n-1} R_X(2h_k)|0\rangle^{\otimes n} = \bigotimes_{k=0}^{n-1} (\cos(h_k)|0\rangle - i \sin(h_k)|1\rangle)$$

Therefore, during the message-passing step, for each edge  $(u, v) \in E$  with classical encodings  $\mathbf{h}_u$  and  $\mathbf{h}_v$ , we prepare the states  $|\phi_{\mathbf{h}_u}\rangle$  and  $|\phi_{\mathbf{h}_v}\rangle$  and apply the edge-local quantum message-passing circuit shown in Figure 3.

Problem (ii) is handled by a simple aggregation procedure. For nodes with multiple neighbors, the message-passing step yields multiple embeddings, one from each incident edge. A unique embedding for each node is obtained by aggregating these embeddings, for example by summation or averaging. Nodes with no neighbors do not participate in the message-passing step, and their embeddings are given directly by the output of the quantum feature extraction procedure.

Algorithm 1 summarizes the full procedure for computing node embeddings.

---

**Algorithm 1** Graph embedding

**Input:** Graph  $G = (V, E)$  with  $|V| = N$ , feature matrix  $X \in \mathbb{R}^{N \times d}$

**Output:** An embedding for each node of  $G$

1. Initialize the list of embeddings  $\mathcal{E}$ .
2. Run the quantum feature extraction to obtain the encodings  $\mathbf{h}_{v_0}, \dots, \mathbf{h}_{v_{N-1}}$  for the nodes in  $G$ .
3. **for**  $(u, v) \in E$  **do**
4.   Prepare the angle encodings  $|\phi_{\mathbf{h}_u}\rangle$  and  $|\phi_{\mathbf{h}_v}\rangle$ .
5.   Run the quantum message passing on the states  $|\phi_{\mathbf{h}_u}\rangle, |\phi_{\mathbf{h}_v}\rangle$ .
6.   Measure the resulting output to obtain embeddings for  $u$  and  $v$ .
7.   Add the embeddings to  $\mathcal{E}$ .
8. **end for**
9. Refine  $\mathcal{E}$  by replacing nodes with multiple embeddings with their sum.

---

### 3.2.4 Trade-off Analysis

The crucial distinction between the edge-local algorithm of Section 3.2.2 and the qubit-efficient version proposed in Section 3.2.3 lies in the trade-off between qubit resources and encoding redundancy.

In the edge-local algorithm of Section 3.2.2, each node is represented by an  $n$ -qubit feature register, requiring a total of  $Nn$  qubits for a graph with  $N$  nodes. This approach allows each node to be encoded at most once, requiring  $O(N)$  angle encodings. However, the hardware requirements scale linearly with the size of the graph, which becomes prohibitive for large graphs on near-term quantum devices.

In contrast, the qubit-efficient edge-local algorithm of Section 3.2.3 constructs a small circuit for each edge  $(u, v)$  using only  $2n$  qubits. This reduces the spatial (qubit) complexity from  $O(Nn)$  to  $O(n)$ , rendering the approach feasible on current quantum hardware regardless of graph size. The trade-off is an increase in encoding redundancy: since a node  $u$  participates in  $\deg(u)$  edges, its feature vector  $\mathbf{h}_u$  must be re-encoded for each incident edge.

Consequently, the total number of angle encoding operations scales as

$$\sum_{u \in V} \deg(u) = 2|E|.$$

For sparse graphs, this increase does not significantly affect the overall computational cost compared to the algorithm of Section 3.2.2. In particular, if the maximum degree of the graph is bounded by a constant, then  $|E| \in O(N)$ , and both algorithms require  $O(N)$  angle encodings.

## 3.3 Deep Graph Infomax Objective

To learn unsupervised node representations, we employ the Deep Graph Infomax (DGI) objective [32], which maximizes

a contrastive lower bound on the mutual information between local node representations and a global summary of the graph.

Let  $\mathcal{H} = \{\mathbf{h}_0, \dots, \mathbf{h}_{N-1}\}$ , where  $\mathbf{h}_j \in \mathbb{R}^d$  for all  $j \in \{0, \dots, N-1\}$ , denote the set of node embeddings produced by Algorithm 1. We first synthesize a global context vector  $\mathbf{s}$  that summarizes the entire graph via a readout function  $f: \mathbb{R}^{N \times d} \rightarrow \mathbb{R}^d$ . In our implementation, we use mean pooling followed by a learnable projection and a sigmoid nonlinearity:

$$\mathbf{s} = f(\mathcal{H}) = \sigma \left( \mathbf{W}_s \cdot \left( \frac{1}{N} \sum_{j=0}^{N-1} \mathbf{h}_j \right) + \mathbf{b}_s \right),$$

where  $\sigma$  denotes the sigmoid activation function and  $\mathbf{W}_s \in \mathbb{R}^{d \times d}$ ,  $\mathbf{b}_s \in \mathbb{R}^d$  are trainable parameters.

The DGI framework employs a discriminator  $D(\mathbf{h}, \mathbf{s})$  that assigns high scores to “true” node-summary pairs and low scores to “false” pairs obtained via a corruption function. Positive samples are given by  $(\mathbf{h}_j, \mathbf{s})$  for  $j \in \{0, \dots, N-1\}$ . Negative samples are generated by applying a corruption operator (in our case, a permutation of the input features) to the graph  $G$ , and then re-running Algorithm 1 to produce corrupted embeddings  $\mathcal{H}' = \{\mathbf{h}'_0, \dots, \mathbf{h}'_{N-1}\}$ . These are paired with the original summary vector to form the pairs  $(\mathbf{h}'_j, \mathbf{s})$ .

We optimize a binary cross-entropy objective over  $N$  positive and  $N$  negative pairs:

$$\mathcal{L}_{\text{DGI}} = -\frac{1}{2N} \sum_{j=0}^{N-1} \left( \log D(\mathbf{h}_j, \mathbf{s}) + \log (1 - D(\mathbf{h}'_j, \mathbf{s})) \right).$$

By optimizing  $\mathcal{L}_{\text{DGI}}$ , the encoder learns node representations that are predictive of the global graph context, encouraging  $\mathcal{H}$  to capture both local structural information and global contextual information.

### 3.3.1 Complexity analysis

In the following, we provide a brief comparison of the running-time complexity of our algorithm with its classical counterpart. We also include the complexity of a *hybrid* algorithm implemented for our experiments (Section 4), which uses the same quantum feature extraction layer as our full quantum model but replaces quantum message passing with a classical message-passing procedure. Throughout this analysis, we assume the number of layers  $L$  is a constant, consistent with our implementation. For classical algorithms, we count the number of elementary arithmetic operations, while for quantum algorithms we count the number of quantum gates.

**Classical GCN.** In a classical GCN, Equation (1), the feature transformation step computes the matrix product  $H^{(l)}W^{(l)}$ , where  $H^{(l)} \in \mathbb{R}^{N \times d}$  and  $W^{(l)} \in \mathbb{R}^{d \times d}$ . This requires  $O(Nd^2)$  operations. The message-passing step multiplies by the normalized adjacency matrix  $D^{-1/2}\tilde{A}D^{-1/2}$ ,

which can be computed in  $O(|E|d)$  operations under the assumption that  $\tilde{A}$  is sparse. The activation function  $\sigma$  is applied componentwise and contributes  $O(Nd)$  operations. Thus, the overall complexity of a classical GCN layer is  $O(Nd^2 + |E|d)$ .

**Quantum algorithm.** In our quantum algorithm (Algorithm 1), the initial amplitude encoding of classical feature vectors into quantum states requires  $O(Nd)$  single-qubit rotations.<sup>1</sup> The quantum feature extraction step applies a fixed quantum circuit of size  $O(\log d)$  to each node. Since this circuit is applied sequentially to all  $N$  nodes, the total gate complexity of this step is  $O(N \log d)$ . The quantum message-passing step iterates over the edges of the graph and applies an edge-local circuit of size  $O(\log d)$  per edge, resulting in a total complexity of  $O(|E| \log d)$ . Combining these contributions, the overall complexity of Algorithm 1 is  $O(Nd + |E| \log d)$ .

**Hybrid algorithm.** In the hybrid algorithm, the initial amplitude encoding and quantum feature extraction steps have complexities  $O(Nd)$  and  $O(N \log d)$ , respectively. The subsequent message-passing step is performed classically and requires  $O(|E| \log d)$  operations. Consequently, the overall complexity of the hybrid algorithm is also  $O(Nd + |E| \log d)$ , matching that of the fully quantum algorithm.

## 4 Experiments

Our experiments are conducted on two datasets: the Cora citation network and a highly differentiated single nucleotide polymorphism (SNP) dataset originally introduced in [37, 24, 5]. In the following, we briefly describe each dataset and explain how the corresponding input graph is constructed in each case.

**SNP Dataset.** The raw dataset consists of  $N = 5008$  haplotypes, each represented by  $d = 805$  binary single nucleotide polymorphism (SNP) features. A haplotype is encoded as a vector  $\mathbf{x} \in \{0, 1\}^d$ , where a value of 1 (resp. 0) at a given coordinate indicates the presence (resp. absence) of a variant allele at the corresponding SNP location.

We construct a graph  $G = (V, E)$  from this dataset as follows. The node set  $V$  consists of all haplotypes. To define the edges, we first compute pairwise cosine similarities between haplotype vectors. Given two nodes  $\mathbf{x}$  and  $\mathbf{y}$ , their similarity is defined as

$$S_{\mathbf{x}\mathbf{y}} = \frac{\langle \mathbf{x}, \mathbf{y} \rangle}{\|\mathbf{x}\| \|\mathbf{y}\|}.$$

To construct the edge set  $E$ , we identify for each node  $\mathbf{x}$  its set of  $k$  nearest neighbors, denoted  $\mathcal{N}_k(\mathbf{x})$ , according to

<sup>1</sup>While the cost of classical-to-quantum data encoding is often ignored in the literature, we explicitly include it here for a fair comparison with classical algorithms.

the similarity scores. In our experiments, we set  $k = 5$ . Unlike standard  $k$ -nearest neighbor graphs, which may give rise to high-degree hubs and oversmoothing in graph neural networks, we employ a *mutual*  $k$ -nearest neighbor construction. Specifically, an undirected edge  $(\mathbf{x}, \mathbf{y})$  is included in  $E$  if and only if

$$(\mathbf{x}, \mathbf{y}) \in E \iff \mathbf{x} \in \mathcal{N}_k(\mathbf{y}) \wedge \mathbf{y} \in \mathcal{N}_k(\mathbf{x}).$$

Finally, to ensure that the resulting graph is connected and captures global structure, we perform a post-processing step to eliminate isolated nodes. For any node with degree zero, we relax the reciprocity constraint and add edges to its  $k$  nearest neighbors. This procedure yields an undirected graph and ensures that rare haplotypes remain connected to the main component, enabling effective message passing.

**Cora Citation Network.** The dataset, which is already presented as a graph, represents academic papers as nodes, each labeled with one of seven research categories, while edges correspond to citation links between papers. Each node is associated with a feature vector given by a bag-of-words (BoW) representation of the paper’s abstract. The dataset contains 2708 nodes, 5429 edges, 1433 features, and seven distinct classes.

### 4.1 Results

To evaluate the learned representations on the SNP dataset, we apply  $k$ -means clustering with  $k = 5$ , motivated by the underlying population structure of the 1000 Genomes dataset, which comprises five super-populations. Although standard internal validation metrics (Silhouette score and the elbow method) suggest an optimal choice of  $k = 3$  or  $k = 4$ —reflecting the substantial genetic overlap between certain continental groups—we adopt  $k = 5$  to align with the known biological taxonomy. The clustering results obtained at  $k = 5$  are nonetheless compelling, as illustrated in Figure 4.

Despite the increased complexity of the task, our model achieves a logistic regression classification accuracy of 98%. This result indicates that our model does not merely recover coarse-grained clusters, but instead learns embeddings that capture fine-grained structure required to distinguish all five super-populations. The slightly lower silhouette score observed at  $k = 5$  compared to  $k = 3$  is expected, as it reflects the inherent genetic proximity between human populations. Nevertheless, the high classification accuracy demonstrates that the learned embedding space preserves sufficient discriminative structure for downstream tasks.

Since the SNP dataset does not provide ground-truth population labels, we adopt a self-supervised evaluation strategy. Rather than comparing against external annotations, we assess the internal consistency and separability of the representations learned by our model. Specifically, we treat the clus-

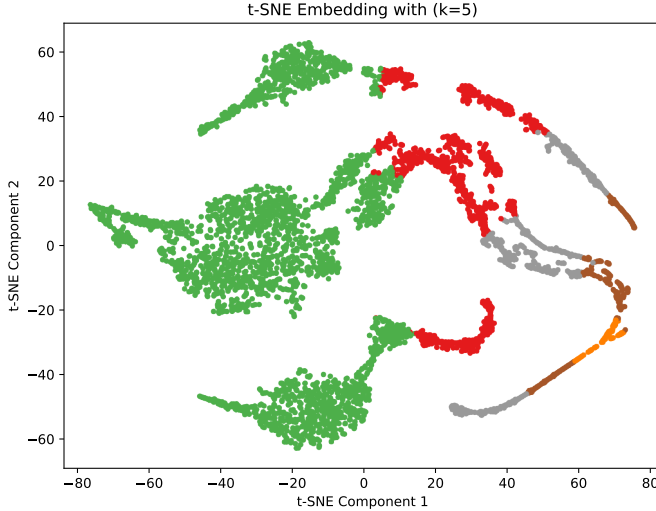


Figure 4: t-SNE embedding visualization of node representations learned by our model on the the SNP dataset.

ter assignments obtained via  $k$ -means clustering with  $k = 5$  as pseudo-labels. We then train a standard logistic regression classifier to predict these pseudo-labels from the embeddings. The resulting high classification accuracy confirms that the learned clusters correspond to linearly separable regions in the embedding space.

To provide a standardized benchmark for the our model, we also conduct experiments on the Cora citation network. While the genetic analysis on the SNP dataset demonstrates the model’s ability to cluster complex, high-dimensional data in an unsupervised setting, the Cora dataset provides ground-truth labels corresponding to seven scientific subject categories. This enables a rigorous evaluation against established real-world classifications and allows us to move beyond self-supervised pseudo-labeling to assess performance using ground-truth metrics.

Furthermore, the NMI score of 0.51 indicates a substantial correspondence between the predicted clusters and the true class distributions, suggesting that the algorithm preserves the semantic structure of the citation graph. Taken together, these results demonstrate that our model is capable of extracting meaningful and separable structure across different domains, regardless of whether ground-truth labels are available during training. Table 1 summarizes the clustering results.

Dataset	Accuracy	Silhouette Score	NMI
SNP	0.98	0.51	N/A
Cora	0.78	0.18	0.51

Table 1: Clustering Results

To rigorously evaluate the contribution of the quantum

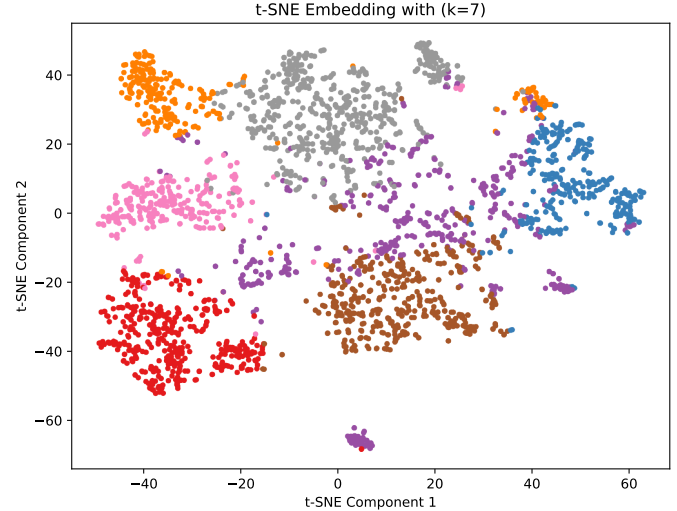


Figure 5: t-SNE embedding visualization of node representations learned by our model on the Cora citation network.

message-passing layer proposed in this work, we compare our architecture against a hybrid model that combines quantum feature extraction with classical message passing. Hybrid quantum-classical models are known to achieve competitive performance in *supervised* classification settings, where ground-truth labels directly guide parameter updates. In contrast, our focus is on the more challenging task of *unsupervised representation learning* using the Deep Graph Infomax (DGI) objective.

On the SNP dataset, both the fully quantum model and the hybrid model exhibit high internal consistency. Similarly, on the Cora citation network, both models achieve high classification accuracy when evaluated against pseudo-labels generated via  $k$ -means clustering. However, this evaluation criterion only verifies that the learned clusters are linearly separable in the embedding space, and does not necessarily indicate semantic alignment with the true class structure.

A clear difference emerges when the learned node embeddings are evaluated against the ground-truth labels of the Cora dataset. The hybrid model attains a Normalized Mutual Information (NMI) score of only 0.06 and a classification accuracy of 0.23, indicating that while the embeddings form well-separated clusters, these clusters exhibit little correspondence with the true research categories. This discrepancy suggests that, in this specific unsupervised setting, classical message passing implemented via linear aggregation (sum) tends to over-smooth the low-dimensional quantum-extracted features, thereby eroding the structural information necessary to recover semantically meaningful labels.

## References

- [1] Xing Ai, Zhihong Zhang, Luzhe Sun, Junchi Yan, and Edwin Hancock. Towards quantum graph neural networks: An ego-graph learning approach. *arXiv preprint arXiv:2201.05158*, 2022.
- [2] Adriano Barenco, Charles H Bennett, Richard Cleve, David P DiVincenzo, Norman Margolus, Peter Shor, Tycho Sleator, John A Smolin, and Harald Weinfurter. Elementary gates for quantum computation. *Physical review A*, 52(5):3457, 1995.
- [3] Kishor Bharti, Alba Cervera-Lierta, Thi Ha Kyaw, Tobias Haug, Sumner Alperin-Lea, Abhinav Anand, Matthias Degroote, Hermanni Heimonen, Jakob S Kottmann, Tim Menke, et al. Noisy intermediate-scale quantum algorithms. *Reviews of Modern Physics*, 94(1):015004, 2022.
- [4] Jacob Biamonte, Peter Wittek, Nicola Pancotti, Patrick Rebentrost, Nathan Wiebe, and Seth Lloyd. Quantum machine learning. *Nature*, 549(7671):195–202, 2017.
- [5] Joseph Bowles. Genomic. <https://pennylane.ai/datasets/other/genomic>, 2025.
- [6] Marco Cerezo, Andrew Arrasmith, Ryan Babbush, Simon C Benjamin, Suguru Endo, Keisuke Fujii, Jarrod R McClean, Kosuke Mitarai, Xiao Yuan, Lukasz Cincio, et al. Variational quantum algorithms. *Nature Reviews Physics*, 3(9):625–644, 2021.
- [7] Samuel Yen-Chi Chen, Tzu-Chieh Wei, Chao Zhang, Haiwang Yu, and Shinjae Yoo. Hybrid quantum-classical graph convolutional network. *arXiv preprint arXiv:2101.06189*, 2021.
- [8] Yi-An Chen and Kai-Feng Chen. Jet discrimination with a quantum complete graph neural network. *Physical Review D*, 111(1):016020, 2025.
- [9] Edward Farhi, Jeffrey Goldstone, and Sam Gutmann. A quantum approximate optimization algorithm. *arXiv preprint arXiv:1411.4028*, 2014.
- [10] Edward Farhi and Hartmut Neven. Classification with quantum neural networks on near term processors. *arXiv preprint arXiv:1802.06002*, 2018.
- [11] Hongyang Gao, Zhengyang Wang, and Shuiwang Ji. Large-scale learnable graph convolutional networks. pages 1416–1424, 2018.
- [12] Justin Gilmer, Samuel S Schoenholz, Patrick F Riley, Oriol Vinyals, and George E Dahl. Neural message passing for quantum chemistry. In *International conference on machine learning*, pages 1263–1272. Pmlr, 2017.
- [13] Stuart Hadfield, Zhihui Wang, Bryan O’gorman, Eleanor G Rieffel, Davide Venturelli, and Rupak Biswas. From the quantum approximate optimization algorithm to a quantum alternating operator ansatz. *Algorithms*, 12(2):34, 2019.
- [14] Will Hamilton, Zhitao Ying, and Jure Leskovec. Inductive representation learning on large graphs. *Advances in neural information processing systems*, 30, 2017.
- [15] Vojtěch Havlíček, Antonio D Cárcoles, Kristan Temme, Aram W Harrow, Abhinav Kandala, Jerry M Chow, and Jay M Gambetta. Supervised learning with quantum-enhanced feature spaces. *Nature*, 567(7747):209–212, 2019.
- [16] Zhirui Hu, Jinyang Li, Zhenyu Pan, Shanglin Zhou, Lei Yang, Caiwen Ding, Omer Khan, Tong Geng, and Weiwén Jiang. On the design of quantum graph convolutional neural network in the nisq-era and beyond. pages 290–297, 2022.
- [17] John Jumper, Richard Evans, Alexander Pritzel, Tim Green, Michael Figurnov, Olaf Ronneberger, Kathryn Tunyasuvunakool, Russ Bates, Augustin Žídek, Anna Potapenko, et al. Highly accurate protein structure prediction with alphafold. *nature*, 596(7873):583–589, 2021.
- [18] Thomas N Kipf and Max Welling. Semi-supervised classification with graph convolutional networks. *arXiv preprint arXiv:1609.02907*, 2016.
- [19] Alex Krizhevsky, Ilya Sutskever, and Geoffrey E Hinton. Imagenet classification with deep convolutional neural networks. *Advances in neural information processing systems*, 25, 2012.
- [20] Ryan LaRose and Brian Coyle. Robust data encodings for quantum classifiers. *arXiv preprint arXiv:2003.01695*, 2020.
- [21] Péter Mernyei, Konstantinos Meichanetzidis, and Ismail İlkan Ceylan. Equivariant quantum graph circuits. In *International conference on machine learning*, pages 15401–15420. PMLR, 2022.
- [22] John Preskill. Quantum computing in the nisq era and beyond. *Quantum*, 2:79, 2018.
- [23] Alec Radford, Karthik Narasimhan, Tim Salimans, Ilya Sutskever, et al. Improving language understanding by generative pre-training. 2018.
- [24] Erik Recio-Armengol, Shahnawaz Ahmed, and Joseph Bowles. Train on classical, deploy on quantum: scaling generative quantum machine learning to a thousand qubits. *arXiv preprint arXiv:2503.02934*, 2025.

[25] Azamat Salamatov and Gowtham Atluri. Quantum and classical graph convolutional neural networks for protein ligand dissociation constant prediction. *bioRxiv*, pages 2025–11, 2025.

[26] Franco Scarselli, Marco Gori, Ah Chung Tsoi, Markus Hagenbuchner, and Gabriele Monfardini. The graph neural network model. *IEEE transactions on neural networks*, 20(1):61–80, 2008.

[27] Michael Schlichtkrull, Thomas N Kipf, Peter Bloem, Rianne Van Den Berg, Ivan Titov, and Max Welling. Modeling relational data with graph convolutional networks. pages 593–607, 2018.

[28] Maria Schuld, Alex Bocharov, Krysta M Svore, and Nathan Wiebe. Circuit-centric quantum classifiers. *Physical Review A*, 101(3):032308, 2020.

[29] Maria Schuld and Francesco Petruccione. Supervised learning with quantum computers. *Quantum science and technology*, 17, 2018.

[30] Maria Schuld and Francesco Petruccione. *Machine learning with quantum computers*, volume 676. Springer, 2021.

[31] Cenk Tüysüz, Carla Rieger, Kristiane Novotny, Bilge Demirköz, Daniel Dobos, Karolos Potamianos, Sofia Vallecorsa, Jean-Roch Vlimant, and Richard Forster. Hybrid quantum-classical graph neural networks for particle track reconstruction. *Quantum Machine Intelligence*, 3(2):29, 2021.

[32] Petar Veličković, William Fedus, William L Hamilton, Pietro Liò, Yoshua Bengio, and R Devon Hjelm. Deep graph infomax. *arXiv preprint arXiv:1809.10341*, 2018.

[33] Guillaume Verdon, Trevor McCourt, Enxhell Luzhnica, Vikash Singh, Stefan Leichenauer, and Jack Hidary. Quantum graph neural networks. *arXiv preprint arXiv:1909.12264*, 2019.

[34] John Watrous. *The theory of quantum information*. Cambridge university press, 2018.

[35] Keyulu Xu, Weihua Hu, Jure Leskovec, and Stefanie Jegelka. How powerful are graph neural networks? *arXiv preprint arXiv:1810.00826*, 2018.

[36] Zi Ye, Kai Yu, and Song Lin. Quantum graph convolutional networks based on spectral methods. *arXiv preprint arXiv:2503.06447*, 2025.

[37] Burak Yelmen, Aurélien Decelle, Linda Ongaro, Davide Marnetto, Corentin Tallec, Francesco Montinaro, Cyril Furtlechner, Luca Pagani, and Flora Jay. Creating artificial human genomes using generative neural networks. *PLoS genetics*, 17(2):e1009303, 2021.

[38] Jin Zheng, Qing Gao, and Yanxuan Lü. Quantum graph convolutional neural networks. In *2021 40th Chinese Control Conference (CCC)*, pages 6335–6340. IEEE, 2021.

[39] Jin Zheng, Qing Gao, Maciej Ogorzałek, Jinhua Lü, and Yue Deng. A quantum spatial graph convolutional neural network model on quantum circuits. *IEEE Transactions on Neural Networks and Learning Systems*, 36(3):5706–5720, 2024.